Coupled internal-state and center-of-mass dynamics of Rydberg atoms in a magnetic guide

M. Traxler,* R. E. Sapiro, K. Lundquist,† E. P. Power, and G. Raithel
Department of Physics, University of Michigan, Ann Arbor, Michigan 48109, USA
(Received 18 March 2013; published 31 May 2013)

We study cold rubidium Rydberg atoms, initially prepared in state $59D_{5/2}$, guided along a two-wire magnetic atom guide. The evolution of the atoms is driven by the combined effects of internal-state transitions and dipole forces acting on the center-of-mass degree of freedom. State-selective field ionization, applied at a variable delay time, is used to investigate the evolution of the internal-state distribution. We observe a broadening of the field ionization spectrum caused by population transfer between Rydberg states. At late times, the distribution of the remaining Rydberg atoms becomes biased toward states with high principal quantum numbers. The population transfer is attributed to thermal transitions and, to a lesser extent, initial state mixing due to Rydberg-Rydberg collisions. Characteristic components in spatially and temporally resolved distributions of the ion signal are interpreted in the context of the underlying physics. The system is simulated with a model in which the center-of-mass dynamics are treated classically, while the internal-state dynamics are treated quantum mechanically. The simulation qualitatively reproduces most experimental findings and provides experimentally inaccessible information.

DOI: 10.1103/PhysRevA.87.053418 PACS number(s): 37.10.Gh

I. INTRODUCTION

Rydberg atoms have been capturing the interest of the scientific community since the 1920s. A variety of traps and guides have been studied for Rydberg atoms: magnetic [1], electrostatic [2], and light field [3] trapping have been experimentally achieved. Theoretically modeled systems include conservative trapping of Rydberg atoms in magnetic guides [4–6] and magnetoelectric trapping of stationary Rydberg atoms [7–10]. We have demonstrated guiding of Rydberg atoms in a linear, high-gradient magnetic atom guide [11]. Trapped Rydberg atoms are of interest in quantum information processing [12], antihydrogen experiments [13–15], and high-precision spectroscopy.

For applications of guided Rydberg atoms, it is necessary to understand their dynamics within the guide, where they interact with their environment and with each other. Conservative magnetic-dipole forces lead to either magnetic trapping or expulsion, depending on the magnetic states of the atoms. The atoms also experience electric-dipole forces in inhomogeneous electric fields. These dipole forces vary in time due to transitions of the atoms between Rydberg levels. Transitions driven by thermal background radiation [16] can add important dynamics, especially in experiments performed in a room-temperature environment. Energy exchange collisions between Rydberg atoms, including Penning ionization, are significant at sufficiently high densities. Penning ionization of Rydberg atoms has been studied elsewhere, experimentally [17,18] and in simulations [19,20]. Radiation- and collision-induced state redistribution effects can be studied using state-selective electric-field ionization [21,22] and microwave ionization [23].

In this paper we analyze collision- and radiation-driven Rydberg atom dynamics in a magnetic guide on a time scale of several milliseconds. In previous work, radiation- and collision-driven internal-state dynamics and center-of-mass evolution of Rydberg atoms in traps have largely been studied independently from each other. In the present work we are considering a system in which the coupling between internal and center-of-mass dynamics represents a major factor in the overall evolution, due to the long duration of the investigated evolution times. In Sec. II we describe the setup of our magnetic guide. The atom dynamics are modeled with a semiclassical Monte Carlo method, which is explained in Sec. III. Time-dependent measurements that reveal the internal-state dynamics of the atoms are presented and discussed in Sec. IV. Conclusions follow in Sec. V.

II. EXPERIMENTAL SETUP

A. Atom guide

The linear magnetic guide is composed of two parallel wires along the z direction. The wires carry equal and parallel currents. This creates a magnetic guide that traps the atoms in the plane transverse to the currents and leaves them free to move in the $+z$ direction, along the symmetry line between the wires. The transverse field gradient is 1.5 kG/cm. The guide carries a beam of ^{87}Rb atoms in the $|F = 1, m_F = -1\rangle$ sublevel of the $5S_{1/2}$ ground state. For details of the guide apparatus see [11,24,25]. The flux of guided ground-state atoms is several 10^7 s^{-1}. The longitudinal temperature is $T_z \approx 1$ mK and the transverse temperature is $T_{x,y} \approx 400$ μK. The average forward velocity of the guided atoms is adjusted to about 1 m/s.

The Rydberg-atom excitation and detection region is located in a long, straight, horizontal section of the magnetic guide. Atoms are optically pumped from the guided ground state $|F = 1, m_F = -1\rangle$ to $F = 2$ with a 780 nm laser that is pulsed on for 10 μs. Then, another pulsed 780 nm laser, on for 5 μs, excites the atoms to the $5P_{3/2}$ $F = 3$ level, from which they are further excited into the Rydberg $59D_{5/2}$ level using a tunable 480 nm laser (which is always on).

*traxlerm@umich.edu
†Present address: Department of Physics, Georgia Institute of Technology, Atlanta, GA 30332.

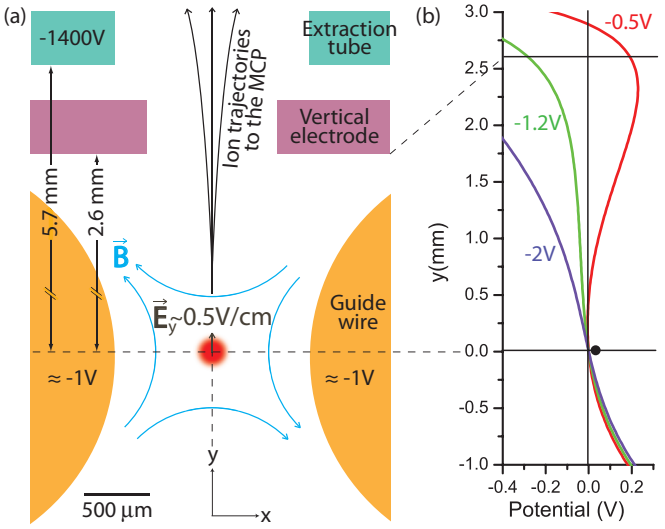

FIG. 1. (Color online) (a) Cross section of the atom-guiding channel and surrounding region. The magnetic field (**B**) is always on and has a minimum at the midpoint between the wires, where the atoms are guided. The electric field at the magnetic-guide minimum points in the y direction and is tuned with the vertical electrode. (b) Electric potential along the y axis, calculated for the three indicated potentials on the vertical electrode.

The magnetic sublevels of $59D_{5/2}$ become approximately equally populated. The Rydberg-atom hyperfine structure is irrelevant. All lasers have a bandwidth of $\sim$1 MHz. The Rydberg atoms are analyzed using state-selective electric-field ionization after a delay time t_d defined as the time between excitation and ionization. Varying t_d allows us to investigate the time evolution of the Rydberg atoms. The freed ions are extracted through the vertical electrode and the extraction tube, shown in Fig. 1, and are imaged onto a microchannel plate (MCP) detector (for details, see [26]). The MCP has a detection efficiency of about 30% for impacting ions.

To field ionize the Rydberg atoms, the potential on the vertical electrode, identified in Fig. 1, is linearly ramped from $\sim$0 V to $-$220 V over a duration of 200 μs beginning at t_d. This corresponds to an electric-field ramp that peaks at 110 V/cm at the location of the atomic beam. At the end of the ramp the electric field is held at the maximum value for 500 μs. The temporal distribution of the state-selective field-ionization (FI) signal is well suited to analyze the internal-state distribution of Rydberg atoms [21,22]. However, the ionization electric field spreads the FI signal ions out in the MCP detector plane, making this method less ideal for spatial analysis. In previous work, we found that microwave ionization produces a spatial distribution that is significantly less dispersed than the FI signal (but largely lacks internal-state resolution). Using microwave ionization, we observed a sample lifetime of about 700 μs, which exceeds the initial state lifetime by about a factor of 5. The increase in lifetime was attributed to internal-state redistribution into long-lived states [11].

We probe the internal-state dynamics of the Rydberg atoms using state-selective FI, with delay times t_d up to 3 ms. The ion counts on the MCP are recorded in two ways, allowing for both temporal and spatial analysis. A multichannel scaler (model SR430) distributes the counts into 2048 time bins. Most multiscaler traces presented here consist of 50 000 averages, except when $t_d \leqslant 500$ μs where we accumulate fewer experimental cycles to avoid saturation of the multiscaler bins. At the same time, the MCP phosphor screen images are recorded with a CCD camera. 30 000 images are averaged, then a background of the same number of images with the guide turned off is subtracted.

B. Electric-field control

Rydberg atoms are extremely sensitive to electric fields, which polarize the atoms and cause electric-dipole forces. The initially excited $59D_{5/2}$ levels exhibit the quadratic Stark effect, and dipole forces scale as $\alpha E \nabla E$, where α is the polarizability and E is the electric-field magnitude. Higher-angular-momentum states, which become populated through thermal transitions and collisions, have permanent dipole moments **p** and dipole forces $(\mathbf{p}\cdot\nabla)\mathbf{E}$. Since these forces may easily overcome the magnetic confinement force in the guide, we must minimize the electric field and its inhomogeneity, throughout the free evolution of the atoms in the guide (i.e., before the time t_d when the FI ramp is applied). Estimates indicate that in the given electrode geometry and for levels in the vicinity of $n = 60$ the electric field must be kept below about 1 V/cm for magnetic guiding to outweigh the electric-dipole forces.

The horizontal electric field E_x is tuned with a potential difference between the guide wires (surface-to-surface separation distance 1.5 mm; see Fig. 1). For $E_x \neq 0$, the ion image on the MCP phosphor screen becomes strongly distorted. By minimizing the distortion we zero E_x to within an uncertainty of 20 mV/cm. This uncertainty is estimated based on the observed sensitivity of the image distortion to the potential difference between the guide wires.

The vertical electric field E_y is harder to estimate and to control than E_x. Figure 1(b) shows that small changes of the potential applied to the vertical electrode produce significantly different electric potentials along the ion extraction trajectory. When the voltage of the vertical electrode is set to values that are more positive than ~-1 V, a potential barrier develops that prevents ions from reaching the MCP, leading to an absence of signal ions originating from within the atom-guiding region. For electrode voltages more negative than ~-2 V, electric-dipole forces increasingly inhibit Rydberg-atom guiding, as evidenced by diminishing ionization signals after about 2 ms. The condition most conducive to Rydberg-atom guiding is found to be an electrode voltage of about -1.2 V [middle curve in Fig. 1(b)], which is used for all data in this paper. With this vertical-electrode potential, the electric field and its inhomogeneity in the atom-guiding region are small enough that electric-dipole forces do not inhibit Rydberg-atom guiding, while the signal ions originating within the atom-guiding region are not blocked from passing through the vertical electrode. An electric-field calculation for this experimental condition shows an electric field of $E_x \approx 0$ and $E_y \approx 0.5$ V/cm at the location of the guiding channel.

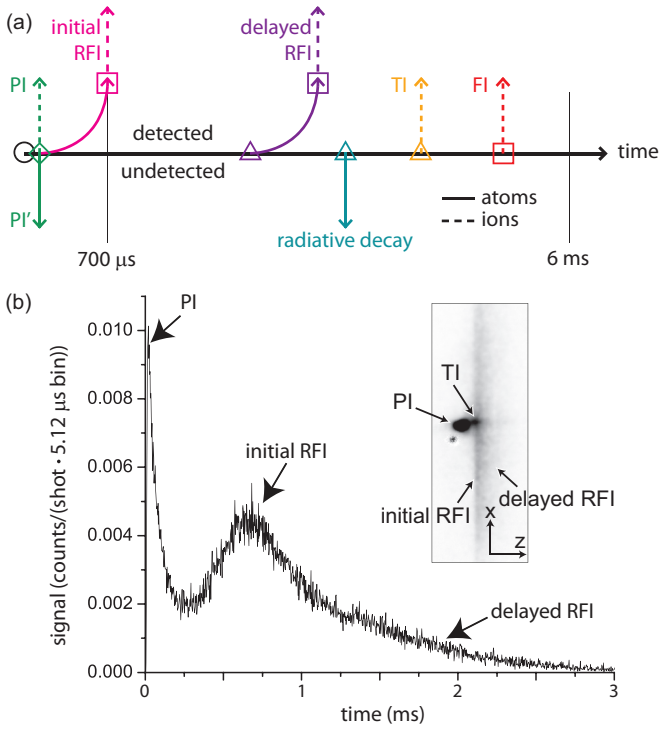

FIG. 2. (Color online) (a) Flow chart of processes affecting Rydberg atoms prepared within a magnetic atom guide, rendered in the (t, y) plane with y as in Fig. 1. Atoms are excited at time $t = 0$. Solid arrows indicate trajectories of bound Rydberg atoms and dashed arrows those of signal ions. Arrows pointing downward indicate atoms that are undetectable. The intrinsic processes, explained in the text, are Penning ionization (PI), initial remote field ionization (RFI), radiative decay, thermal ionization (TI), and delayed remote field ionization. Field ionization (FI) is the only applied process. FI is applied at t_d, which we vary from 5 μs to 3 ms. The symbols indicate atom-field interactions, namely, laser excitation from the ground state (◯), Rydberg-Rydberg collisions (◇), interaction with thermal photons (△), and ionization in a quasistatic electric field (□). (b) Multiscaler trace for the free evolution signal with an applied electric field of $E_y = 0.6$ V/cm. The inset shows the corresponding image.

III. OVERVIEW OF PROCESSES

Since signals from a number of different processes are superimposed in the ion images and in the multiscaler traces, the analysis of the Rydberg-atom evolution in the guide is nontrivial. It is necessary to use both temporal (multiscaler traces) and spatial (ion images) information to understand the processes involved. In the ion images, the z axis correlates directly with time since the Rydberg atoms move at about 1 m/s along z. The flowchart in Fig. 2(a) provides a concise summary of the relevant processes, while Fig. 2(b) shows a free-evolution multiscaler trace and corresponding ion image illustrating the signal produced by each process.

At the excitation time [denoted by ◯ in Fig. 2(a)], samples of ∼100 Rydberg atoms are prepared within the atom-guiding region, which, for ground-state atoms, is a cylindrical tube of several 100 μm diameter that is concentric with the symmetry axis between the guide wires. About half of the initially excited Rydberg atoms are in high-magnetic-field-seeking states, and are expelled from the guide. A fraction of those move up along the y direction, approach the strong electric field present in the slit in the vertical electrode, become field ionized (□ in Fig. 2), and produce a signal that we refer to as the initial remote field ionization (RFI) signal. The initial RFI signal is widely dispersed in the x direction because the points of origin of the corresponding ions are spread out across the x width of the slit in the vertical electrode; the initial RFI signal shows up as the left edge of the long vertical streak in the ion image in Fig. 2(b). The arrival time of the initial RFI signal at the MCP is governed by the time it takes for expelled Rydberg atoms to move close to the vertical electrode, where they ionize; the additional time of flight of the ions to the MCP is negligible. The initial RFI signal begins to rise at about 300 μs and peaks at about 700 μs after excitation in the multiscaler trace in Fig. 2(b).

The initial Rydberg atom density is sufficiently high that Penning ionization (PI) also occurs [◇ in Fig. 2(a)] [27]. PI′ denotes the atoms that are deexcited to lower n values in the Penning collisions, thereby becoming undetectable in our system. The production rate of PI ions is highest immediately after excitation. Because the ion time of flight from the atom-guiding location (symmetry axis between the guide wires) to the MCP is only on the order of a few tens of microseconds, the PI signal peaks almost immediately in the multiscaler trace in Fig. 2(b). The PI signal ends at ∼200 μs after excitation; after that time the sample density becomes so low that PI ceases. Further, the PI ions, which all originate from within the atom-guiding region, are imaged into a tight, concentrated spot in the ion images. Because of the presence of PI, we expect that other state-changing, nonionizing collisions (ℓ and n mixing [18,28,29]) also occur within the system during these early times in the evolution.

The most important interaction affecting the internal states of the guided Rydberg atoms is with the 300 K thermal radiation [△ in Fig. 2(a)]. The thermal effects are, in decreasing order of importance, bound-bound transitions into nearby Rydberg states, thermal ionization, and thermally enhanced radiative decay into low-lying atomic states. The Rydberg atoms that radiatively decay into low-lying atomic states are not detected. Rydberg atoms present in the guide also produce a weak ionization current due to thermal ionization [TI in Fig. 2(a)]. This signal is so weak that it cannot be discerned in the multiscaler traces. However, since TI ions are generated near the atom-guiding channel, the corresponding signal in the ion images is quite concentrated (similar to the PI signal) and can be discerned in Fig. 2(b). The simulation, explained in Sec. IV, shows an overall TI probability per atom of approximately 7%.

Guided Rydberg atoms continue to interact with thermal radiation, and transitions of guided Rydberg atoms into magnetically unguided states continue to occur at decreasing rates until no Rydberg atoms are left. Atoms that are guided for some time and then transition into a high-magnetic-field-seeking state follow a path similar to that of the atoms causing the initial RFI signal. The resultant RFI signal is delayed by the amount of time the atoms were actually guided. It shows up in the multiscaler traces as a long tail past the initial RFI peak; in the ion images the RFI signal is widely spread out

along x and located to the right of the initial RFI signal [see Fig. 2(b)].

The electric-field ionization ramp, applied at a variable time delay t_d, causes the FI ion signal. The temporal distribution of the FI signal over the duration of the FI ramp allows us to determine the internal-state distribution of the Rydberg atoms. The FI signal is the only signal discussed here that is not caused by the free evolution of the Rydberg atoms in the guide. When applied, the FI ionizes all remaining Rydberg atoms, creating a very strong signal that dominates in the multiscaler traces and the ion images. The ions giving rise to the FI signal originate from within the atom-guiding region, like the PI and TI signal ions. However, since the FI ions are subject to the strong electric field of the FI ramp, the imaging conditions are substantially different. Unlike the PI and TI signals, the FI signal is spread out in the x direction. By moving the excitation location and tracking the FI signal on the MCP, the x magnification of the FI signal is measured to be $M_x = 6.6$. The x spread of the RFI signal looks similar to that of the FI signal. However, the x magnification of the initial and delayed RFI signals are hard to define and cannot be measured because both types of signal ions originate in an extended region away from the atom-guiding region and close to the vertical electrode. Due to the finite size of the MCP, the wings of the FI and both types of RFI signals are slightly cropped.

IV. SIMULATION METHOD

Before proceeding to a discussion of the internal-state distribution in our system, we first present a simulation to model the internal-state and center-of-mass dynamics. We simulate the experiment by treating the atoms' center-of-mass dynamics classically and using a quantum Monte Carlo method for their internal-state evolution. The Rydberg atoms are in well-defined $|n,\ell,j,m_j\rangle$ states at each time step of the simulation. The quantization axis for each atom is given individually by the direction of the magnetic field at that atom's location. Given that the center-of-mass oscillation frequency within the guide is in the kHz range and the Zeeman splittings are in the MHz range, we assume that changes in magnetic-field direction are followed adiabatically by the internal states of the atoms, leading to well-defined m_j values and atomic g factors at all times. At each time step, the probabilities of thermally induced transitions into other bound target states with $5 \leqslant n' \leqslant 100$ or free target states with energy $\epsilon' \leqslant 0.25$ eV are calculated for a radiation temperature of 300 K. All possible radiative electric-dipole transitions are taken into account. Random numbers determine if the atoms remain in their current states or undergo a quantum jump. The simulated quantum jumps are photoionization ($|n,\ell,j,m_j\rangle \rightarrow |\epsilon',\ell',j',m'_j\rangle$ with free-electron energy ϵ') and transitions into different Rydberg states ($|n,\ell,j,m_j\rangle \rightarrow |n',\ell',j',m'_j\rangle$). Since the detailed electron properties after photoionization are irrelevant, photoionization is simulated as one quantum-jump channel, which is a sum over all unbound target states. For the bound-bound quantum jumps there are hundreds of channels, one for each relevant target state. Taking into account the known probabilities for the various jumps, a random number determines whether a quantum jump occurs and which one it is. After each quantum jump, the affected atom emerges in a well-defined new state (or is flagged as photoionized or decayed). The time step size is dynamically adjusted so that the total quantum-jump probability does not exceed a few percent per time step.

The model accounts for lifetime increases by thermally driven transitions into states with higher n, ℓ, and m_j; atom loss due to thermal photoionization; decay toward the ground state; and radiatively driven transitions from positive m_j (atoms guided) to negative m_j (atoms magnetically expelled from the guide). The simulation is initialized with all atoms having well-defined (n,ℓ,j)-quantum numbers and randomly selected m_j values. The magnetic force, given by the internal-state m_j values and g factors, acts on the center-of-mass coordinates of the atoms. The internal-state dynamics lead to time-dependent $m_j(t)$, which are different for each realization of an internal-state quantum trajectory. The functions $m_j(t)$ determine the atoms' center-of-mass trajectories in the inhomogeneous guide magnetic field, which are computed classically.

In the experiment, we observe an initial phase ($\lesssim 200$ μs) of Penning ionization ($\diamond$ in Fig. 2). This observation suggests some degree of n-, l-, and m-mixing of the remaining, non-Penning-ionized atoms during this initial period. However, during most of the evolution time the system is collision-free due to low densities and thermal transitions are the main driver of the evolution. We expect that initial collisions do not have a strong effect on the internal-state and center-of-mass dynamics, and we therefore do not include collisions in the simulation. Such an extension of the simulation could possibly be implemented in the future. An initial phase of state-mixing collisions, which would coincide in time with the Penning ionization phase, may explain why the fraction of Rydberg atoms left at late times is larger than expected from a collision-free model by a factor on the order of 10 [11].

V. TEMPORAL DATA AND INTERNAL-STATE DYNAMICS

The manifestations of the signal components corresponding to intrinsic processes have already been discussed in Sec. III. For reference, the free-evolution case is shown in Fig. 2(b) and is repeated by the gray trace in Fig. 3.

Due to the long evolution time in our system and the fact that the guide operates at room temperature, the most important interaction of the Rydberg atoms is the interaction with background blackbody radiation [30–32]. Thermal transitions within the bound-state space of the Rydberg atoms cause a diffusionlike behavior in all quantum numbers, as well as thermal ionization. Collisions play a role in the internal-state distribution of the Rydberg atoms, as well. We have estimated that $\sim$10% of the Rydberg atoms are Penning ionized [11], which implies that another $\sim$10% are transferred into lower-n states due to Penning collisions. The Penning ionization rate is dependent on Rydberg-atom density ($\sim 2 \times 10^{14}$ m^{-3}), thermal velocity (on the order of 0.4 m/s), and collision cross sections (on the order of 2×10^{-12} m^2 for $n = 59$). Using these values and noting the amount of time during which the sample is relatively dense (on the order of 100 μs), we estimate Penning ionization probabilities that are in line with our experimental observations. With our time resolution it is impossible to distinguish between rapid (submicrosecond) ionization and

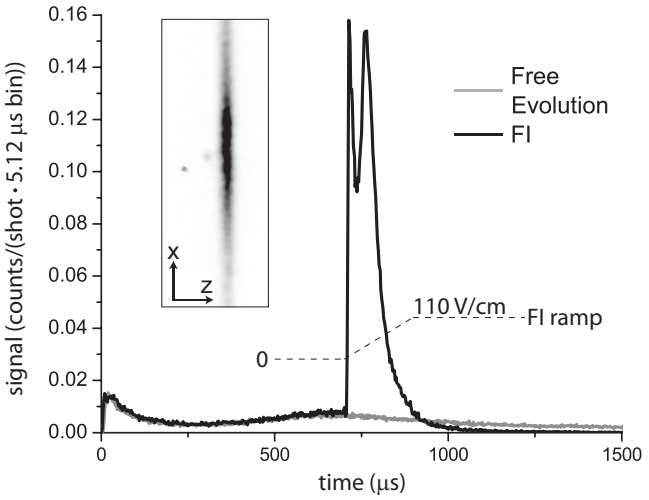

FIG. 3. Multiscaler trace for FI (black) for $t_d = 700\ \mu$s, compared to free evolution (gray). The inset shows the corresponding FI image.

PI events picking up after a few microseconds of motion (such a distinction was made in an experiment in Ref. [33]). Due to energy conservation, the principal quantum number of the product atoms [PI′ in Fig. 2(a)] must be less than $n_0/\sqrt{2}$, where n_0 is the initial principal quantum number. The product atoms are out of range of the state-selective field-ionization ramp that is applied to obtain the FI signal. The experimentally observed presence of Penning ionization suggests that other nonionizing, n-changing and ℓ-changing collisions are also present in the system during the first $\lesssim$100 μs.

In order to study the internal-state distribution of the Rydberg atoms resulting from thermal and collisional processes as a function of evolution time, we apply a field-ionization ramp after a delay time t_d. This delay time is varied from 5 μs to several milliseconds. A typical trace of an FI signal, with $t_d =$ 700 μs, is shown by the black curve in Fig. 3 along with the corresponding ion image. The applied field ionization ionizes all of the Rydberg atoms in the guide, thus terminating the free evolution; all Rydberg atoms in the guide at t_d contribute to the FI signal. By integrating the FI signal and comparing it to the integral of the free evolution signal, we see that the signal yield due to FI is about three times that due to RFI.

Since the rise time of the applied field-ionization ramp is fairly long (200 μs) the distribution of counts along the time axis in the multiscaler traces allows us to extract the distribution of ionization electric fields of the Rydberg atoms present in the guide. To compare simulated with experimental data, the raw simulated distributions $p(n)$ after evolution time t_d are mapped into distributions

$$\tilde{p}(E) = p(n)\left|\frac{dn}{dE}\right| = p(n(E)) \times 4n^5,$$

where E is the ionization field, $E = \frac{1}{16n^4}$. Further, for the given linear electric-field ramp the simulated distribution vs time is $\tilde{p}(t_R) = (dE/dt_R)\tilde{p}(E(t_R))$. There, t_R is defined as the time elapsed after the start of the FI ramp.

The FI signal in Fig. 3 exhibits two peaks that appear during the FI ramp. Figure 4(a) zooms into this region of interest, showing FI traces for several t_d, while Fig. 4(b) shows corresponding simulated FI traces, $\tilde{p}(t_R)$, taken from simulated n distributions at the given t_d. The experimental data in Fig. 4(a) is normalized to the second peak, which occurs at $t_R \approx 60\ \mu$s and does not depend on t_d.[1] The simulated

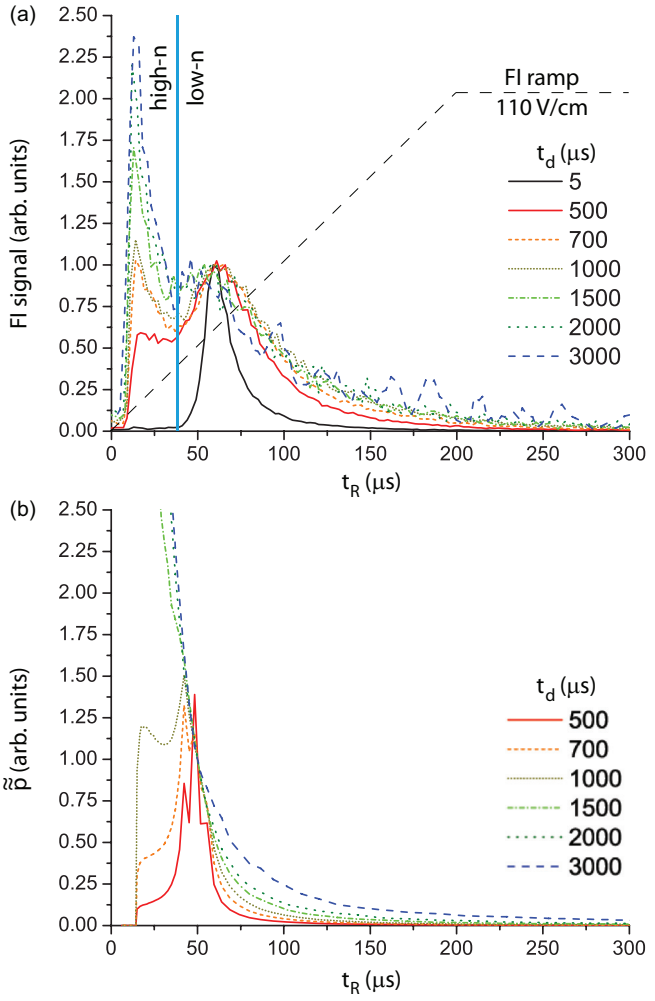

FIG. 4. (Color online) (a) Experimental FI data. Each multiscaler trace is normalized to the height of the second peak. The field-ionization ramp (dashed line) is superimposed with the multiscaler traces. The vertical blue line marks the valley between the two peaks. (b) Corresponding FI curves, $\tilde{p}(t_R)$, derived from the simulated n distributions at different t_d. In both (a) and (b), the curves for $t_d = 3000\ \mu$s have been smoothed by adjacent averaging.

[1]The FI signal does not develop any diabatic field-ionization signature that would typically be expected from Rydberg atoms transitioning into higher-angular-momentum states [22]. The absence of diabatic FI is a reasonable, if unexpected, observation. Our FI ramp is quite slow, making the FI process more adiabatic. A possibly stronger reason for the lack of diabatic peaks is that, as seen in Fig. 1(a), once an atom is slightly above the center of the guiding channel it enters a region where the magnetic field is transverse to the ionization electric field. This magnetic field is on the order of tens of Gauss and couples states with m-quantum numbers different by 1; coupling strengths scale as 1.4 MHz/G. Therefore, the magnetic

data in Fig. 4(b), meanwhile, is normalized at $t_R = 50\ \mu$s, in approximate correspondence with the normalization applied to the experimental data. There is a slight discrepancy in the timing of the peaks compared with the experimental data, which we attribute to the fact that the simulation does not take into consideration the ion times of flight. The second peak corresponds to the field-ionization signature that arises from atoms in the initial state ($59D$) and other nearby states. By around $t_d = 2$ ms (1.5 ms in the simulated data), the field-ionization signature of the initial-state population diminishes into a shoulder and, at even later times, becomes increasingly insignificant when compared to the first peak. The dominant first peak is indicative of a transfer of a large fraction of Rydberg atoms into states with n much higher than the initial-state principal quantum number.

The two plots in Fig. 4 allow us to obtain insight into the evolution of the n-state distribution of the atoms. As the value of t_d increases, the low-n peak broadens due to Rydberg atoms transitioning into higher and lower principal quantum states, driven by thermal radiation transitions, and, in the first $\sim 100\ \mu$s, probably also by state-changing collisions. In the experimental data, this broadening is mostly complete by $t_d \geqslant 1$ ms, after which time the low-n side becomes form invariant, indicating that the relative $n < n_0$-state distribution has become fixed. By about $t_d = 700\ \mu$s in the data and $t_d = 1$ ms in the simulation, a prominent first peak arises, due to accumulation of Rydberg atoms in states with high principal quantum number. These states have longer lifetimes than the initially populated $59D$ and so tend to accumulate in higher proportions at long times; in addition, due to the n^5 factor on the right-hand side of the equation above, the atoms in a range of high-n states become field ionized in rapid succession at the very beginning of the field-ionization ramp. This leads to the dominance of the first peak at larger t_d. In the simulation, the high-n peak near $t_R = 0$ keeps rising even at longest values of t_d. This is not the case in the data, where the high-n peak reaches a relative steady state at about 2 ms. We attribute this difference to the E_y electric field, which is present in the experiment but not in the simulation. The higher the n value of an atom, the higher the likelihood that the electric field pulls the atom from the guide due to electric-dipole forces. Apparently, in the experiment a relative, dynamic steady-state between high-n atoms being pulled from the guide and atoms transitioning into these same states is reached at about 2 ms.

The increase in average n corresponds to a decrease in the average ionization electric field. Specifically, we can calculate the electric field that corresponds to the minimum between the two peaks in Fig. 4(a). This minimum (marked with a vertical blue line in the figure at $t_R = 36\ \mu$s, corresponding to $n = 64$) represents a convenient experimental dividing point between the high-n and low-n states.

For the values of t_d used in Fig. 4, the fraction of Rydberg atoms in states with $n \gtrsim 64$, $F_{\text{high}}(t_d)$, is obtained by integrating the multiscaler traces from $t_R = 0$ to $t_R = 36\ \mu$s in the experiment and dividing by the integral over the entire t_R range. In the simulation, we obtain $\sum_{n\geqslant 64} p(n)/\sum_{n\geqslant 20} p(n)$.

field turns crossings into anticrossings in the Stark maps, pushing the system toward adiabatic FI.

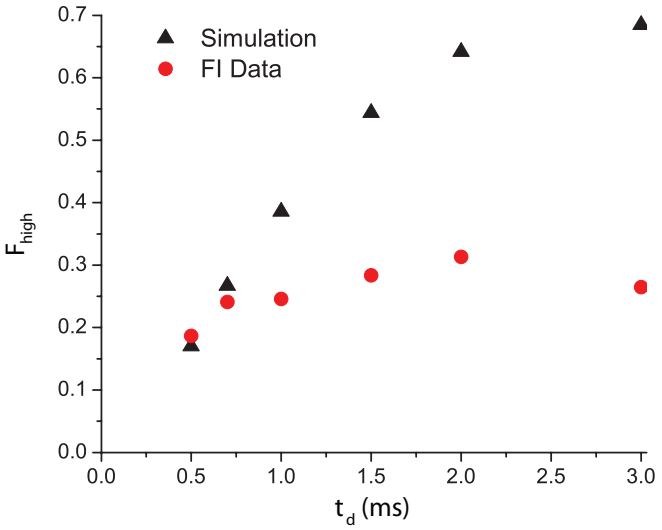

FIG. 5. (Color online) Fraction of high-n state atoms, F_{high}, as a function of t_d. Both experiment and simulation show that thermal transitions cause an accumulation of population in higher-n states. In the experiment, the trend saturates at a lower value, presumably due to electric-dipole forces that increase in n and limit the accumulation of trapped-atom population.

Measured and simulated values of $F_{\text{high}}(t_d)$ are compared in Fig. 5. The statistical uncertainties of the FI data are smaller than the plotted dots; systematic uncertainties in the experimental data due to laser intensity, frequency, and atomic-beam density drifts are estimated at several percent. Figure 5 demonstrates that $F_{\text{high}}(t_d)$ increases both in experiment and simulation; the simulated value is consistently higher than the experimental one. In the experiment F_{high} levels off at about 30% at long times, whereas in the simulation it reaches 70%. The discrepancy is likely due to the E_y electric field, which leads to a saturation of the experimentally observed high-n fraction at a lower value.

The simulation allows additional insights that are not available in the experiment. Simulated internal-state dynamics for ℓ and m_j as a function of time are shown in Fig. 6. Figure 6(a) shows that both the average ℓ value, ℓ_{avg}, and the width of the ℓ distribution increase with time. The distribution starts with an initial ℓ value of 2, corresponding to the initial $59D$ state. By $t_d = 6$ ms, it ends with $\ell_{\text{avg}} \approx 7$. This increase in ℓ_{avg}, along with the simultaneous increase in n, explains the long lifetimes that are seen experimentally [11].

The m_j values, which are initialized in the simulation to random values, spread both positively and negatively at early times. Atoms with $m_j < 0$ are high-field seeking and are magnetically expelled from the guide. A fraction of these atoms become directed into regions of high electric-field strength, where they ionize and give rise to the initial RFI signal. Thus, after $t_d \approx 500\ \mu$s, the average value of m_j shifts higher as seen in Fig. 6(b). Atoms with positive m_j tend to maintain a positive m_j for some time, since the diffusive radiative transport in m space is quite slow. The probability flow rate from the magnetically guided ($m_j > 0$) into the magnetically expelled ($m_j < 0$) domain diminishes with increasing time, as indicated by the arrows in Fig. 6(b).

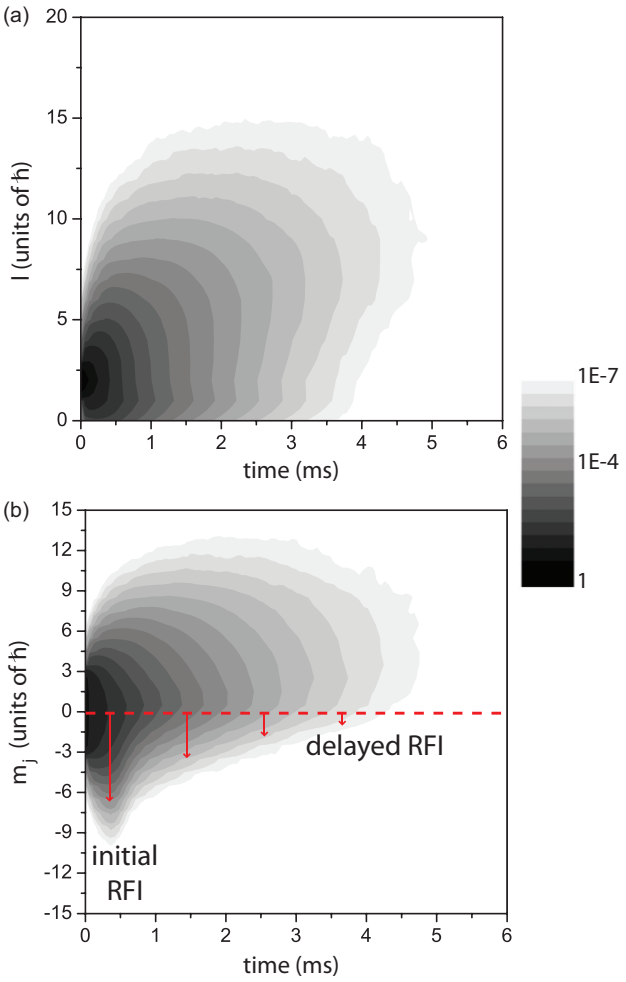

FIG. 6. (Color online) Simulated internal-state dynamics as a function of time. (a) ℓ distribution. (b) m_j distribution. The broadening of the distributions is driven by thermal transitions. Atoms driven into $m_j < 0$ states depart from the guide, giving rise to the RFI signal. The length of the arrows indicates the departure rate.

The probability flow from positive to negative m_j gives rise to the delayed RFI signal. Most of the remaining atoms have positive m_j values by the end of the simulated time.

VI. CONCLUSIONS

We have investigated the coupled internal-state and center-of-mass dynamics of Rydberg atoms in an atom guide over several milliseconds, using FI and simulations as our tools. We find that atoms move toward higher n, higher ℓ, and higher m_j over time, mostly due to thermal transitions. These contribute to the previously observed long lifetimes in our guide [11]. Several intrinsic processes occur due to the coupled internal-state and center-of-mass dynamics (PI, initial and delayed RFI, TI).

Rydberg atom guides as described in this paper may offer new opportunities in several areas. It is possible to initialize the atoms into circular Rydberg levels using an adiabatic state-switching method. The crossed-field method [34], which is compatible with various types of atom guides (magnetic, electric, optical), would enable the preparation of a cold, slow beam of guided circular Rydberg atoms. Circular Rydberg atoms have low susceptibility to stray electric fields and long lifetimes (tens to hundreds of milliseconds in a 4 K environment), making them ideal for cavity-QED experiments with superconducting microwave resonators [35–37]. A guided, cold beam of such atoms may enable new studies in this area, in quantum information transport and processing with Rydberg atoms (see, e.g., [38]), and possibly in high-precision spectroscopy [39,40].

ACKNOWLEDGMENTS

This work has been supported by the Army Research Office (50396-PH) and in part by the National Science Foundation (PHY-0855871). Equipment purchased with a DURIP grant (No. FA550-10-1-0371) was used. M.T. acknowledges support by a National Defense Science and Engineering Graduate fellowship.

[1] J.-H. Choi, J. R. Guest, A. P. Povilus, E. Hansis, and G. Raithel, Phys. Rev. Lett. **95**, 243001 (2005).
[2] S. D. Hogan and F. Merkt, Phys. Rev. Lett. **100**, 043001 (2008).
[3] S. E. Anderson, K. C. Younge, and G. Raithel, Phys. Rev. Lett. **107**, 263001 (2011).
[4] I. Lesanovsky, J. Schmiedmayer, and P. Schmelcher, Phys. Rev. A **70**, 043409 (2004).
[5] I. Lesanovsky, J. Schmiedmayer, and P. Schmelcher, Europhys. Lett. **65**, 478 (2004).
[6] I. Lesanovsky and P. Schmelcher, Phys. Rev. Lett. **95**, 053001 (2005).
[7] B. Hezel, I. Lesanovsky, and P. Schmelcher, Phys. Rev. Lett. **97**, 223001 (2006).
[8] U. Schmidt, I. Lesanovsky, and P. Schmelcher, J. Phys. B: At., Mol. Opt. Phys. **40**, 1003 (2007).
[9] M. Mayle, I. Lesanovsky, and P. Schmelcher, Phys. Rev. A **80**, 053410 (2009).
[10] M. Mayle, B. Hezel, I. Lesanovsky, and P. Schmelcher, Phys. Rev. Lett. **99**, 113004 (2007).
[11] M. Traxler, R. E. Sapiro, C. Hempel, K. Lundquist, E. P. Power, and G. Raithel, Phys. Rev. A **86**, 023414 (2012).
[12] D. Jaksch, J. I. Cirac, P. Zoller, S. L. Rolston, R. Côté, and M. D. Lukin, Phys Rev. Lett. **85**, 2208 (2000).
[13] A. Speck, C. H. Storry, E. A. Hessels, and G. Gabrielse, Phys. Lett. B **597**, 257 (2004).
[14] F. Robicheaux, Phys. Rev. A **73**, 033401 (2006).
[15] G. B. Andresen *et al.* (Alpha Collaboration), Nat. Phys. **7**, 558 (2011).
[16] M. R. Flannery and D. Vrinceanu, Phys. Rev. A **68**, 030502(R) (2003).

[17] J. O. Day, E. Brekke, and T. G. Walker, Phys. Rev. A **77**, 052712 (2008).
[18] A. Walz-Flannigan, J. R. Guest, J.-H. Choi, and G. Raithel, Phys. Rev. A **69**, 063405 (2004).
[19] F. Robicheaux, J. Phys. B: At., Mol. Opt. Phys. **38**, S333 (2005).
[20] S. D. Chao, M. Hayashi, S. H. Lin, and E. W. Schlag, J. Phys. B: At. Mol. Opt. Phys. **31**, 2007 (1998).
[21] Thomas F. Gallagher, *Rydberg Atoms* (Cambridge University Press, Cambridge, 1994).
[22] R. F. Stebbings and F. B. Dunning, *Rydberg States of Atoms and Molecules* (Cambridge University Press, Cambridge, 1983).
[23] J. G. Leopold and I. C. Percival, Phys. Rev. Lett. **41**, 944 (1978).
[24] S. E. Olson, R. R. Mhaskar, and G. Raithel, Phys. Rev. A **73**, 033622 (2006).
[25] R. R. Mhaskar, S. E. Olson, and G. Raithel, Eur. Phys. J. D **41**, 221 (2007).
[26] V. D. Vaidya, M. Traxler, C. Hempel, R. R. Mhaskar, and G. Raithel, Rev. Sci. Instrum. **81**, 043109 (2010).
[27] R. Stephen Berry, Radiat. Res. **59**, 367 (1974).
[28] S. K. Dutta, D. Feldbaum, A. Walz-Flannigan, J. R. Guest, and G. Raithel, Phys. Rev. Lett. **86**, 3993 (2001).
[29] A. Reinhard, T. Cubel Liebisch, K. C. Younge, P. R. Berman, and G. Raithel, Phys. Rev. Lett. **100**, 123007 (2008).
[30] E. J. Beiting, G. F. Hildebrandt, F. G. Kellert, G. W. Foltz, K. A. Smith, F. B. Dunning, and R. F. Stebbings, J. Chem. Phys. **70**, 3551 (1979).
[31] T. F. Gallagher and W. E. Cooke, Appl. Phys. Lett. **34**, 369 (1979).
[32] W. E. Cooke and T. F. Gallagher, Phys. Rev. A **21**, 588 (1980).
[33] P. J. Tanner, J. Han, E. S. Shuman, and T. F. Gallagher, Phys. Rev. Lett. **100**, 043002 (2008).
[34] D. Delande and J. C. Gay, Europhys. Lett. **5**, 303 (1988).
[35] G. Raithel, C. Wagner, H. Walther, L. Narducci, and M. Scully, *Cavity Quantum Electrodynamics*, edited by Paul Berman (Academic, New York, 1994).
[36] S. Haroche, AIP Conf. Proc. **464**, 45 (1999).
[37] J. M. Raimond, M. Brune, and S. Haroche, Rev. Mod. Phys. **73**, 565 (2001).
[38] M. Saffman, T. D. Walker, and K. Mølmer, Rev. Mod. Phys. **82**, 2313 (2010).
[39] J. Hare, A. Nussenzweig, C. Gabbanini, M. Weidemuller, P. Goy, M. Gross, and S. Haroche, IEEE Trans. Instrum. Meas. **42**, 331 (1993).
[40] R. Lutwak, J. Holley, P. P. Chang, S. Paine, D. Kleppner, and T. Ducas, Phys. Rev. A **56**, 1443 (1997).